Solid State Sciences 83 (2018) 99–106

Contents lists available at ScienceDirect

Solid State Sciences

journal homepage: www.elsevier.com/locate/ssscie

Enhancement of photovoltaic performance of polyaniline/graphene composite-based dye-sensitized solar cells by adding TiO_2 nanoparticles

Kailash Nemade[a,*], Priyanka Dudhe[b], Pradip Tekade[b]

[a] Department of Physics, Indira Mahavidyalaya, Kalamb 445 401, India
[b] Department of Chemistry, Jankidevi Bajaj College of Science, Wardha 442 001, India

ARTICLE INFO

Keywords:
Photovoltaic
Polyaniline
Graphene
TiO_2

ABSTRACT

Polyaniline (PANi)-graphene composites and polyaniline-graphene/TiO_2 composites were prepared by ex-situ approach. Systematic investigation was carried out to explore photovoltaic (PV) properties of PANi-graphene and PANi-graphene/TiO_2 composite. The prepared composites were characterized using X-ray diffraction (XRD), Scanning Electron Microscope (SEM), Raman Spectroscopy and Ultraviolet–Visible (UV–Vis) Spectroscopy. The PV properties of dye-sensitized solar cells (DSSCs) prepared composites investigated by assembling materials in ITO/PANi-graphene/Al and ITO/PANi-graphene/TiO_2/Al architecture. Different PV parameters such as short circuit current, open circuit voltage, fill factor and power conversion efficiency were determined from the (Current-Voltage) IV characteristics of PV cell. The 15 wt% PANi loaded graphene composite based PV cell shows optimized power conversion efficiency of the order 6.47%. The main accomplishment of present work is that efficiency associated with 15 wt% PANi loaded graphene composite, improved further by addition of TiO_2 nanoparticles. The composite system between PANi-graphene/TiO_2 for 1 wt% of TiO_2 nanoparticles shows optimized power conversion efficiency of the order 8.63%.

1. Introduction

Global demand of energy rising gradually, due to heavy industrialization and urbanization. Developed countries have huge demands of energy while demand is going on increasing in developing countries. The International Energy Agency states that energy needs are projected to expand by 55% till 2030 [1]. But unfortunately, the complete demand of energy is satisfied through non-renewable energy sources such as coal, petroleum, and natural gas. The exploitation of non-renewable energy sources results in range of adverse effects like air and water pollution, damage to public health, global warming and unnecessary atmospheric changes. Key solution for this issue is to use renewable energy sources such as hydropower, geothermal, wind and solar energy instead of non-renewable energy sources. Among these renewable energy sources, solar energy is best option due to outstanding characteristics such as the most abundant, inexhaustible and clean of all the renewable energy resources till date.

Across the globe researchers takes great interest in identification of alternative materials to silicon. The downside associated with silicon-based photovoltaic (PV) cell technology is their manufacturing requires costly ultra-high-purity silicon. Also, this process of manufacturing of PV cell results in significant carbon emission. Organic materials are considered as close competitive and alternative to the standard silicon-based PV cell technology. The main causes behind the development of organic PV cell technology are less expensive, thinner, more flexible, and amenable to a wide range of lighting conditions. Another interesting reason is low material consumption results in a high absorption coefficient [2]. Some other advantages of organic PV cells are low specific weight, mechanical flexibility, tunable material properties and high transparency [3].

During literature survey on organic PV materials, we come across three efficient materials which exhibits outstanding PV properties. These three materials are polyaniline, graphene and TiO_2 nanoparticles. Among the conducting polymers such as polyaniline (PANi), polypyrrole (PPy) and polythiophene (PTh), PANi has been extensively studied by researchers.

Conducting polymer is the class of materials, which is fit for photovoltaic application and device fabrication. This is because of outstanding characteristics such as intrinsically stable photoexcitation with visible light, high photon harvesting efficiency, tunable band gap engineering on the entire visible spectral range and large charge generation when mixed with electron acceptor materials [4].

PANi display good electron conducting behaviors, interesting redox behavior, high environmental stability and controllable electrical and

* Corresponding author.
E-mail address: krnemade@gmail.com (K. Nemade).

https://doi.org/10.1016/j.solidstatesciences.2018.07.009
Received 9 May 2018; Received in revised form 14 July 2018; Accepted 16 July 2018
Available online 17 July 2018

optical properties [5–7]. All these outstanding features of PANi attributed to the delocalized π-electron structure. The optical absorption coefficient of organic molecules specially in case of PANi is very high. Therefore, large amount of light can be trap by an insignificant amount of materials [8].

Graphene possesses a substantial number of wonderful optical and electronic properties, such as zero band-gap, semi-conducting with a high carrier mobility and high optical transparency, which generally not observed in other materials [9]. It is well accepted principle for organic PV cells that optimization of both charge transport and optical properties are necessary for good performance.

Out of many semiconducting metal oxides, TiO_2 has some attractive features for PV cell application. TiO_2 nanomaterial suitable for PV cell application due to its high chemical and optical stability, non-toxicity, low cost, corrosion resistance and ease of synthesis [10,11]. Many reports show that graphene–TiO2 nanocomposites possess superior photovoltaic properties than pristine TiO_2 [12].

The composite preparation using organic and inorganic constituent's results in improved electronic properties. It is well known principle of materials science that in synergetic state, physical and chemical properties of most of the composite improves. Therefore, in this section it is analyzed using some reports on PV properties of PANi-Metal Oxide composite. The addition of metal oxides impurity in PANi enhance the PV properties and increase the efficiency of solar cells.

Ameen et al. fabricated TiO_2/PANi and dye absorbed TiO_2/PANi electrodes by plasma polymerization for solar cells application. The results of the study indicate that dye absorbed TiO_2/PANi electrode based DSSCs have high charge carrier transportation between the TiO_2 and PANi layer. This rapid charge transportation in dye absorbed TiO_2/PANi electrode improves the performance of solar cell than the TiO_2/PANi electrode [13]. Shen et al. architecture PV cell with layers ITO/nano-crystalline TiO_2/PANi/Aluminum. This shows largest open voltage of 0.397 V and short current density of 65.9 μA/cm^2 under simulated solar radiation. Using current-voltage characteristics, the formation of p-n junction between nano-crystalline TiO_2 and PANi interface is also verified [14]. Yang et al. synthesized grafted aniline on aminobenzoate monolayer to adsorbed TiO_2 nanocrystal to fabricate a uniform core/shell structured TiO_2/PANi nanocomposite. The DSSC fabricated with an electrode of TiO_2/PANi film have considerably high short circuit current density of 0.19 mA/cm^2 and an open circuit voltage of 0.35 V [15]. Zhu et al. adopted the two-step process to prepared PANi hybridized ZnO photoanode on FTO substrate. The results of the study show that light-conversion efficiency of PANi hybridized ZnO nanograss improves by 60% than pure ZnO nanograss photoanode [16]. Momeni et al. studied the dye-sensitized solar cell based on TiO_2 nanotube arrays. In this work, TiO_2 nanotubes were prepared by two different approaches namely one-step and two-step process. This work concludes that TiO_2 nanotubes prepared using two-step process shows higher efficiency [17]. Bahramian et al. prepared in situ PANi-based counter electrode and coral-likeTiO_2 to assemble DSSC with transparent PANi films as counter electrode. This bifacial DSSC have power conversion efficiency of 8.22%, which is assigned to excellent light scattering by the coral-like TiO_2 and high specific surface area of PANi nanofibers [18]. Duan et al. fabricated the DSSC with PANi incorporated TiO_2 anodes, PANi counter electrodes, and iodide doped PANi solid-state electrolytes. The results of the study show that DSSC with proper assembly process and iodide dosage provides good PV performances with power conversion efficiency of 3.1% [19].

The humankind has been gifted by many brilliant materials by nature, one of those is Graphene. Graphene possess noticeable enigmatic optical and electronic properties such as zero band gap, high carrier mobility, high optical transparency. The synergetic phase of graphene with PANi, also results in efficient PV materials. Some reports on PANi-Graphene composite have been reviewed in this section.

Wang et al. prepared graphene/PANi nanocomposite by polymerization of aniline monomer in situ method. In DSSC, graphene/PANi nanocomposite deposited on FTO, which gives power conversion efficiency of 6.09% compared to 6.88% of efficiency for PV cell with expensive Pt counter electrode under similar experimental conditions [20]. Liu et al. designed DSSC by coating a nanocomposite thin film of graphene/PANi on FTO glass by electro-polymerization method. In comparison, graphene/PANi based electrode has power conversion efficiency of 7.17%, which is close to 7.24% of a DSSC with a Pt counter electrode. This study shows that graphene/PANi electrode has potential to replace conventional Pt counter electrode in DSSC [21]. Dinari et al. designed the Pt free DSSC using PANi-Graphene quantum dots by in situ electrochemical polymerization on FTO coated glass. The synergistic effect between PANi and graphene quantum dots provides higher electrochemical catalytic activity which resulted into improved PV performance with power conversion efficiency of 1.6% [22].

Loryuenyong et al. fabricated DSSCs with counter electrode based on PANi-graphene hybrid material. The counter electrode was prepared by depositing material on FTO by drop casting method. The PANi/graphene hybrid counter electrode exhibits superior PV performance with open circuit voltage of 0.57 V, Short Circuit Current of 5.15 mA cm^{-2}, fill factor of 0.40 and power conversion efficiency of 1.16% which results in improved PV performance than DSSC based on Pt electrode [23]. Yang et al. synthesized multilayer counter electrodes from positively charged PANi-graphene complex and negatively charged platinum nanoparticles with different number of layers and different concentration of graphene in PANi-graphene complex. This work concludes that the electron migration from graphene to PANi helped in good charge transfer. This multilayer interface based DSSC has power conversion efficiency of 7.45%. This work also pointed that multi-interfacial counter electrodes are suitable for robust DSSC [24].

During literature survey, it is observed that PANi, TiO_2 nanoparticles and Graphene have much potential to improve their PV properties. The necessity of development of new kinds of PV materials with improved power conversation efficiencies is being touched by different research groups across the globe. Therefore, the problem is identified on the basis of following remarks:

- During study, it is observed that concentration of impurity in composite has play crucial role. Therefore, in this work it planned to investigate optimized composition of PV material based on PANi and graphene.
- In second step, after successful finding of optimized composition, another impurity that is TiO_2 used for further enhancement of PV properties of PANi-graphene composite.

Therefore, the objectives of present work are to prepare and optimized PV properties of PANi-graphene composite. Then prepare and optimized TiO_2 nanoparticles loaded PANi-graphene composite for PV application.

2. Experimentation

2.1. Preparation of materials

2.1.1. Preparation of PANi

In the present work, PANi was synthesized by using chemical oxidative method. In this method, ammonium persulfate was used as an oxidizing agent. All chemicals required for the preparation of PANi procured from SD fine, India of AR grade and used without further purification. In the process of preparation of PANi, following steps were executed,

- During the synthesis of PANi, one condition is imposed on molar ratio between ammonium persulfate to aniline monomer should not exceed the ratio ≤1.15. The reason behind this condition is to obtain high conductivity and yield [25].
- With this condition, both aniline monomer and ammonium

persulfate dissolve separately in aqueous (100 ml) medium.
- Subsequent to this step, the solution of aniline monomer was added in ammonium persulfate solution in dropwise manner under magnetic stirring.
- The greenish-black precipitate was observed in beaker with increase in temperature.
- This precipitate was kept for overnight (24 h) for good quality polymerization.
- On next day, precipitate was washed three times with distilled water to remove un-reacted contents in product.
- The obtained product was dried at 50 °C and used for further process.

2.1.2. Preparation of PANi/Graphene composites

The *ex-situ* approach was adopted for the preparation of PANi/Graphene composite. The graphene required for the composite preparation was prepared by previously reported method [26]. The weight % (wt.%) stoichiometry was adopted for the preparation of composites. The wt.% stoichiometry was calculated using relation (Eq. (3.1)),

$$wt.\ \% = \frac{A}{(A+B)} \times 100 \tag{3.1}$$

where A and B are constituents of composite.

In our case, the content of PANi in composite was varied for 5–20 wt % by an interval of 5 wt%. In this way, four samples were obtained. During preparation of composite, both constituents of composite was added in 25 ml acetone under magnetic stirring at room temperature.

2.1.3. Preparation of PANi/graphene-TiO_2 composites

PANi/Graphene-TiO_2 composites was also prepared by ex-situ approach. In this process, TiO_2 was directly procured from SD fine, India of high purity. This TiO_2 was probe sonicated using sonicator (PCi, 750-F, PCI Analytics Pvt Ltd). This process of probe sonication, splits the TiO_2 particles up to the nano-dimensions. As-obtained TiO_2 nanoparticles, was used for the preparation of composites. By adopting wt.% stoichiometry, four samples of PANi/Graphene-TiO_2 composites were prepared by varying content of TiO_2 nanoparticles in composite from 0.5 to 2 wt% by an interval of 0.5 wt%. The optimized stoichiometry between PANi and graphene were used further for addition of TiO_2 nanoparticles, to improve PV properties. Here also, acetone was used as an organic media for the preparation of composites. For dye sensitization process, Ru-based N719 dye was used by preparing media of 0.25 mM ethanolic solution of dye N719.

2.2. Fabrication of photovoltaic cell

The doctor blade technique was used to fabricate the PV cells. During this process, the composites was sandwiched between cleaned ITO plate as transparent electrode and Aluminum electrode. The aluminum foil was used as metallic electrode for the PV cell. ITO plate (Dimension: 25 mm × 25 mm) used in this work was procured from Techinstro (ITO-SE-011), India. With the help of temporary binder (based on 3% ethyl cellulose and 97% butyl digol), composite was deposited on ITO electrode and then Aluminum electrode was deposited. This fabricated cell allows to dry at 40 °C for 3 h for evaporation of volatile organic compounds. The thickness of deposited layer controlled by thickness of transparency used during doctor blade technique. In this way, PV cells were fabricated for further study. The side face of fabricated PV cell is depicted in Fig. 1.

2.3. Measurements of photovoltaic characteristics

The current-voltage (IV) characteristics of PV cell collected under incandescent light bulb of power 0.2956 Watt/m^2. The separation between incandescent light source and PV cell was about 15 cm. The important diode parameters like open circuit voltage (V_{OC}), short circuit current (I_{SC}), fill factor (FF), and power conversion efficiency (η) were measured under these conditions, which reproduced without any considerable deviation. The FF of PV cell computed using relation Eq. [1] [27]:

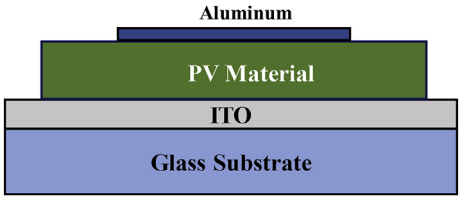

Fig. 1. Side face of fabricated PV cell.

$$FF = \frac{I_{MAX} \times V_{MAX}}{I_{SC} \times V_{OC}} \tag{1}$$

Whereas, power conversion efficiency (%η) of PV cell estimated using the relation Eq. [2]. [28],

$$\%\eta = \left(\frac{I_{SC} \times V_{OC} \times FF}{P_{in}}\right) \times 100 \tag{2}$$

The FF and %η are the crucial parameters for any PV cell. On the basis of these parameters, it is possible to discriminate any PV cell and its performance.

3. Results and discussion

3.1. Materials characterization and PV properties of PANi/Graphene

3.1.1. XRD analysis

Fig. 2 (a) shows the XRD pattern of pure PANi synthesized by chemical oxidative method. The XRD pattern of pure PANi comprises only one broad peak around 26°, which indicates the poor crystallinity phase of PANi. This broad peak is also assigned to the scattering from the PANi chains at inter planar spacing [29]. Fig. 2 (b) depicts XRD pattern of graphene, which has well structural, and phase purity. The XRD of graphene possesses two signature peaks at 26.3° (002) and 44.2° (100). The peak at 2θ = 26.3° indicates well organized structure of graphene with an interlayer spacing of 0.339 nm. This layer spacing is

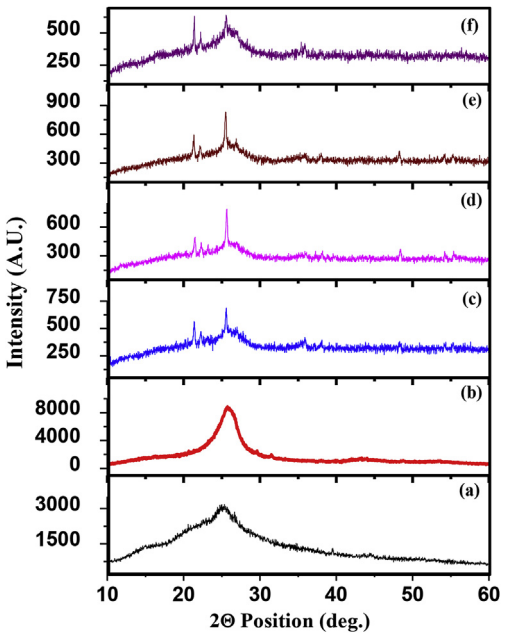

Fig. 2. XRD pattern of pure (a) PANi, (b) graphene and (c) 5 wt%, (d) 10 wt%, (e) 15 wt%, (f) 20 wt% PANi loaded graphene composites.

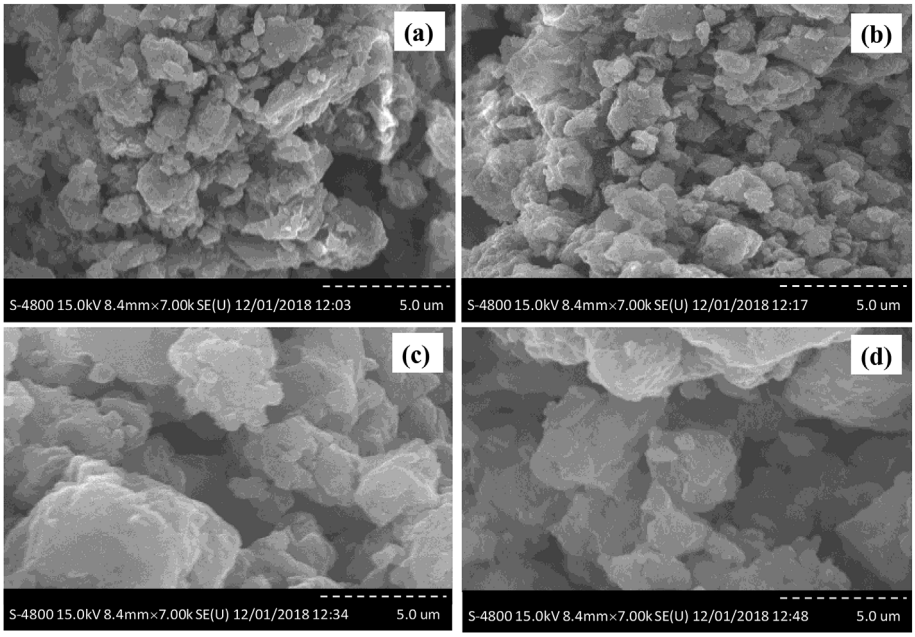

Fig. 3. SEM images of (a) 5 wt%, (b) 10 wt%, (c) 15 wt% and (d) 20 wt% PANi loaded graphene composites.

in agreement with spacing in graphite. The broad peak at 2θ = 44.2° is attributed to presence of some defects [30]. Fig. 2 (c, d, e and f) shows the XRD pattern of 5 wt%, 10 wt%, 15 wt% and 20 wt% PANi loaded graphene composites, respectively. XRD pattern shows that with an increase in PANi content in composites, noisy behavior of pattern increases. This indicates that crystalline nature of composites decreases. Sharp peaks appear between 20 and 26° is attributed to the presence of smaller crystalline regimes in composites. The decrease in peak height intensity of composites than graphene and PANi, justify the formation of composites.

3.1.2. Morphology study

Fig. 3 shows the SEM images of (a) 5 wt%, (b) 10 wt%, (c) 15 wt% and (d) 20 wt% PANi loaded graphene composites prepared by ex-situ approach. In all cases, graphene sheets are homogeneously dispersed in PANi. At fixed resolution, one thing is observed from SEM images that agglomeration phenomenon increases with wt.% of PANi. All composite samples have irregular shape.

3.1.3. Raman Spectroscopy

Fig. 4 depicts the Raman spectra of 15 wt% PANi loaded graphene composite, which is optimized sample in PV study. The C – N stretching vibration from benzenoid structure appears through band 1548 cm^{-1}. The semi-benzenoid polaronic band of $C–N^{+}$ appears at 1318 cm^{-1} and plane bending vibration of CH is appears at 1200 cm^{-1}. The Raman spectrum comprises clear band D (1325 cm^{-1}) [31], G (1598 cm^{-1}), and 2D (2695 cm^{-1}), which are signature band of graphene [32–34]. The shift in band position is observed, which is attributed to the structural changes in resultant composite. The quinoid rings in the PANi have a similar atomic structure with the C6 rings of graphene. This situation in both constituents allow for a strong π -π stacking interaction and beneficial for electronic transmission [35].

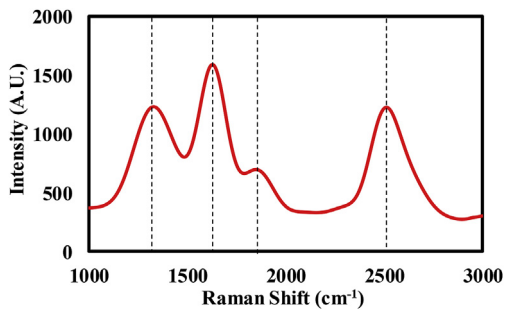

Fig. 4. Raman spectrum of 15 wt% PANi loaded graphene composite.

3.1.4. Optical properties

In PV technology, optical properties of PV materials play crucial role. Therefore, in our case it is studied using UV-VIS spectroscopy. In PV cell technology, both types of band gap materials that is low-band gap and high-band gap materials have their own importance. Therefore, by combining appropriate materials to obtain band gap which efficiently used available solar radiations is necessary. This is necessary, if the band gap is very small than incident photon energy, then considerable photon energy converted in heat energy, which raise the temperature of PV materials. On other hand, if the band gap is very large, it restricts the transition between valance band to conduction band [36].

Fig. 5 shows the UV-VIS spectrum of 5 wt%, 10 wt%, 15 wt% and 20 wt% PANi loaded graphene composites. From plot, it is clearly

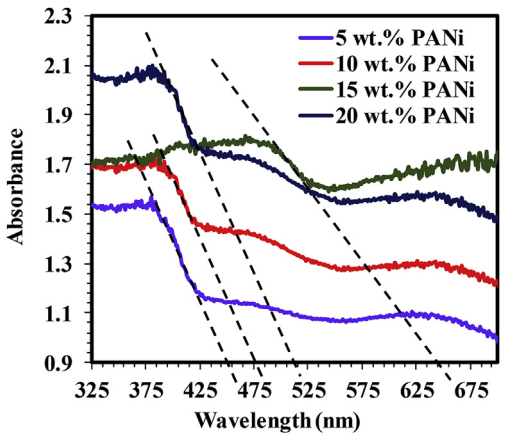

Fig. 5. UV-VIS spectrum of 5 wt%, 10 wt%, 15 wt% and 20 wt% PANi loaded graphene composites.

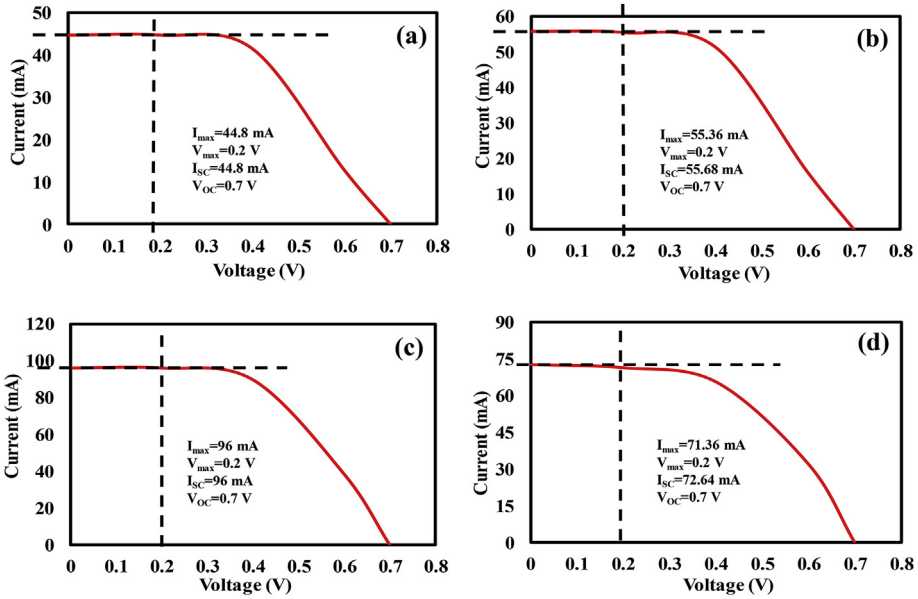

Fig. 6. PV response of (a) 5 wt%, (b) 10 wt%, (c) 15 wt% and (d) 15 wt% PANi loaded graphene composite.

observed that the samples 5 wt%, 10 wt% and 20 wt% PANi loaded graphene composites have absorption tail at lower wavelength than 15 wt% PANi loaded graphene composites. The band gap values for as-prepared composite samples (estimated using frequency-wavelength relation) ranges between 2.73 and 1.92 eV. The lowest value of band gap is associated with 15 wt% PANi loaded graphene composite.

3.1.5. PV performance

Fig. 6 shows the PV response of (a) 5 wt%, (b) 10 wt%, (c) 15 wt% and (d) 15 wt% PANi loaded graphene composite based DSSCs. All diode parameters like I_{max}, V_{max}, I_{SC}, V_{OC}, FF and %η are provided in Table 1. Among all PV cells, the response of 15 wt% PANi loaded graphene composite has highest power conversion efficiency of order 6.479% (FF = 0.285). The highest power conversion efficiency was attributed to lower band gap value (1.92 eV) of 15 wt% PANi loaded graphene composite. All samples have stable diode parameters and reproducible results.

Fig. 7 shows the variation of FF and %η as a function wt.% of PANi in composite. Plot shows that 15 wt% PANi loaded graphene composite has highest power conversion efficiency. The possible reason for highest power conversion efficiency may be

Table 1
PV parameters of TiO_2 nanoparticles loaded PANi-graphene composites and PANi loaded graphene composites.

TiO_2 nanoparticles loaded PANi-graphene composite						
Wt.% of TiO_2 nanoparticles	I_{max} (mA)	V_{max} (V)	I_{SC} (mA)	V_{OC} (V)	FF	%η
0.5 wt%	95.17	0.2	95.23	0.8	0.2499	6.43
1 wt%	127.71	0.2	127.79	0.8	0.2498	8.63
1.5 wt%	106.59	0.2	106.65	0.8	0.2498	7.21
2.0 wt%	105.73	0.2	105.8	0.8	0.2498	7.15
PANi loaded graphene composite						
Wt.% of PANi	**I_{max} (mA)**	**V_{max} (V)**	**I_{SC} (mA)**	**V_{OC} (V)**	**FF**	**%η**
5 wt%	44.8	0.2	44.8	0.7	0.285	3.068
10 wt%	55.36	0.2	55.68	0.7	0.284	3.741
15 wt%	96	0.2	96	0.7	0.285	6.479
20 wt%	71.36	0.2	72.64	0.7	0.280	4.816

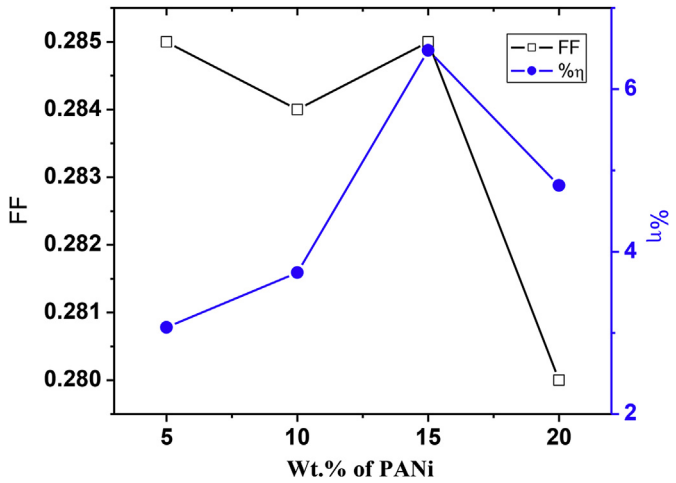

Fig. 7. Variation of FF and %η as a function wt.% of PANi in composite.

- the homogeneous presence of PANi and graphene in composite, can reduce the interfacial resistance between the graphene and the PANi. This homogeneity in composite results in better electron transfer.
- The presence of high electrical conductive graphene in composite and agglomerated nature of composite reduce inter-domain resistance.
- Lower band gap (1.92 eV) value of 15 wt% PANi loaded graphene composite.

3.2. Improvement in PV performance by addition of TiO_2 nanoparticles

3.2.1. XRD analysis

Fig. 8 (a) shows the XRD pattern of anatase phase TiO_2 nanoparticles. The strong signature peaks at 25° and 48° confirms the anatase phase. All remaining peaks position and marginal intensity data are in good agreement with standard spectrum (JCPDS card No. 84–1286) [37]. The average crystallite size of TiO_2 nanoparticles was estimated using Scherrer equation [38], $D = (K\lambda/\beta\cos\theta)$, where D is average crystallite size (nm), k is a shapes factor (K = 0.89), λ is the wavelength of X-ray source equals 1.540 Å, β is the full width at half maxima, and θ is the diffraction peak angle. The average crystallite size of TiO_2

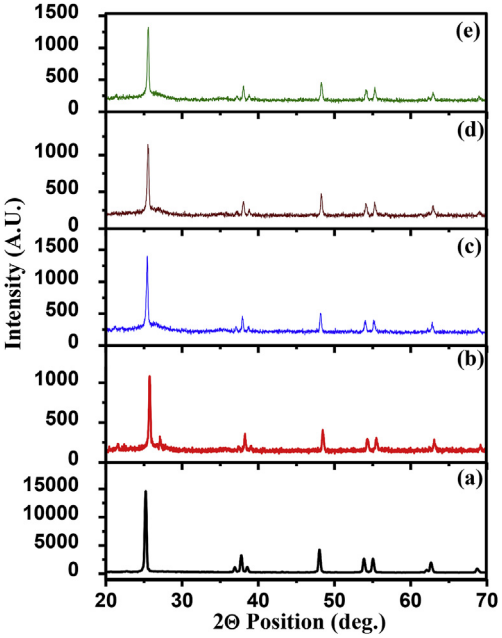

Fig. 8. XRD pattern of pure (a) TiO_2 nanoparticles and (b) 0.5 wt%, (c) 1 wt%, (d) 1.5 wt% and (e) 2 wt% TiO_2 nanoparticles loaded PANi-graphene composites.

nanoparticles was found to be 51.27 nm. Fig. 8 (b, c, d and e) depicts the XRD pattern of 0.5 wt%, 1 wt%, 1.5 wt% and 2 wt% TiO_2 nanoparticles loaded PANi-graphene composites, respectively. The addition of TiO_2 nanoparticles in PANi-graphene composites results in interesting results. The XRD pattern clearly shows the composite exhibits the crystalline phase with shape peaks. As discussed in section 4.1.1, the PANi-graphene composites have amorphous phase, which was diminish by addition of TiO_2 nanoparticles.

3.2.2. Morphology study

Fig. 9 represents the SEM images of (a) 0.5 wt%, (b) 1 wt%, (c) 1.5 wt% and (d) 2 wt% TiO_2 nanoparticles loaded PANi-graphene composites. Here also, TiO_2 nanoparticles nicely dispersed in PANi-graphene composites. The addition of TiO_2 in PANi-graphene results in improvement of crystallinity. In all SEM images, well defined crystalline boundaries are observed. The crystallinity of all composite samples reflects also from XRD analysis. The irregular particle size distribution observed in all regions of SEM.

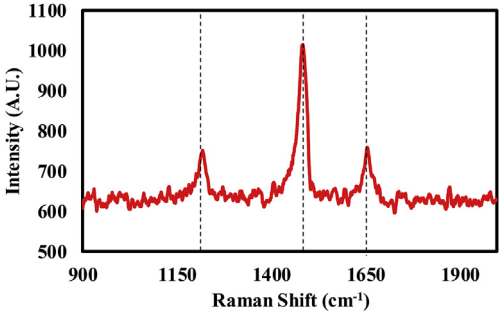

Fig. 10. Raman spectrum of 1 wt% TiO_2 nanoparticles loaded PANi-graphene composite.

3.2.3. Raman Spectroscopy

Fig. 10 shows the Raman spectrum of 1 wt% TiO_2 loaded PANi-Graphene composite. This spectrum also comprises the C−N stretching vibration from benzenoid, which appears around 1548 cm^{-1}. Similarly, semi-benzenoid polaronic band of $C–N^+$ appears around 1318 cm^{-1} and plane bending vibration of C-H is appears around 1200 cm^{-1}. No significant peaks were associated with TiO_2 nanoparticles in spectrum.

3.2.4. Optical properties

Fig. 11 shows the UV-VIS spectrum of 0.5 wt%, 1 wt%, 1.5 wt% and 2 wt% TiO_2 nanoparticles loaded PANi-graphene composites. From the plot, it is clear that absorption tail of 1 wt% TiO_2 nanoparticles loaded PANi-graphene composite has higher value than other three samples. The band gap values of 0.5 wt%, 1 wt%, 1.5 wt% and 2 wt% TiO_2 nanoparticles loaded PANi-graphene composites ranges between 3.02 and 2.53 eV. The lowest value of band gap is associated with 1 wt% TiO_2 nanoparticles loaded PANi-graphene composite.

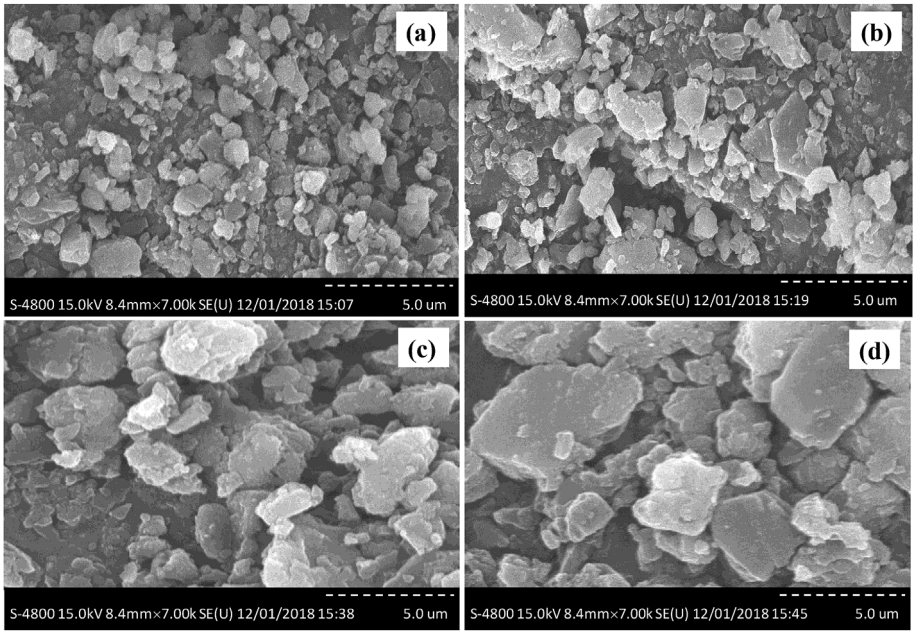

Fig. 9. SEM images of (a) 0.5 wt%, (b) 1 wt%, (c) 1.5 wt% and (d) 2 wt% TiO_2 nanoparticles loaded PANi-graphene composites.

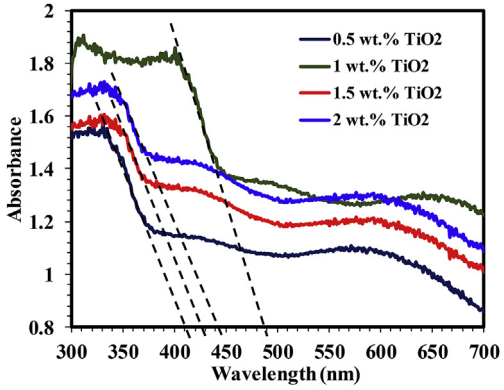

Fig. 11. UV-VIS spectrum of 0.5 wt%, 1 wt%, 1.5 wt% and 2 wt% TiO_2 nanoparticles loaded PANi-graphene composites.

3.2.5. PV performance

Fig. 12 shows the PV response of (a) 0.5 wt%, (b) 1 wt%, (c) 1.5 wt% and (d) 2 wt% TiO_2 nanoparticles loaded PANi-graphene composites based DSSCs and all diode parameters listed in Table 1. In PANi-graphene/TiO_2 composite, stable diode parameters observed. From Table 1, it is observed that 1 wt% TiO_2 nanoparticles loaded PANi-graphene composite has highest power conversion efficiency. The highest power conversion efficiency was attributed to good optical properties and lower band gap (2.53 eV) value.

Fig. 13 depicts the variation of FF and %η as a function wt.% of TiO_2 nanoparticles in PANi-graphene composites. The highest power conversion efficiency was associated with 1 wt% of TiO_2 nanoparticles in PANi-graphene composite. The possible reasons for the highest power conversion are,

- The addition of TiO_2 nanoparticles in PANi-graphene composite, results in increase of both photocurrent density and open circuit voltage.
- The presence of graphene sheets in composite reduces charge recombination and increasing open circuit voltage as a result of high electron [39,40].

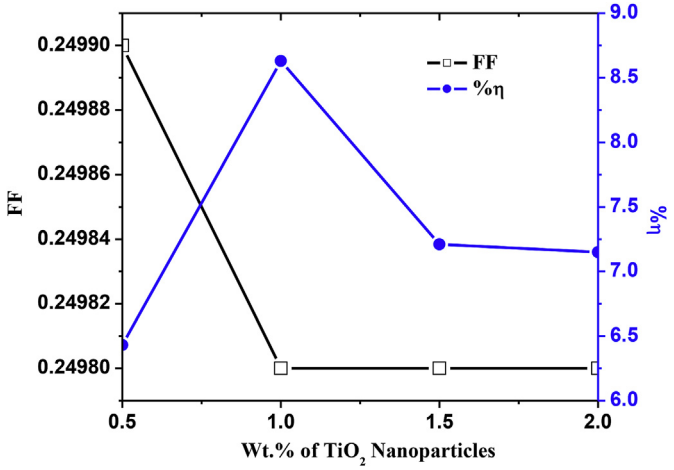

Fig. 13. Variation of FF and %η as a function wt.% of TiO_2 nanoparticles in composites.

4. Conclusions

During the study, two material systems that is PANi-graphene composite and PANi-graphene/TiO_2 composites based DSSCs were successfully prepared by ex-situ approach. The structural, morphological and optical study of both systems were carried out to understand physical properties of materials. To analyze the PV performance of PANi-graphene composite and PANi-Graphene/TiO_2 composites, PV cells were fabricated using doctor blead technique in architecture ITO/PV materials/Aluminum.

The PANi required for composite preparation was synthesized by using chemical oxidative route successfully. During composite preparation wt.% of PANi varied in graphene, to analyze effect of PANi on PV properties of composite. In this study, 15 wt% PANi loaded graphene composite shows optimized power conversion efficiency of order 6.47% with I_{sc} = 96 mA. The highest power conversation efficiency of this sample attributed to reduction in the interfacial resistance between the graphene and the PANi, lower inter-domain resistance and lower band gap of 15 wt% PANi loaded graphene composite than other samples.

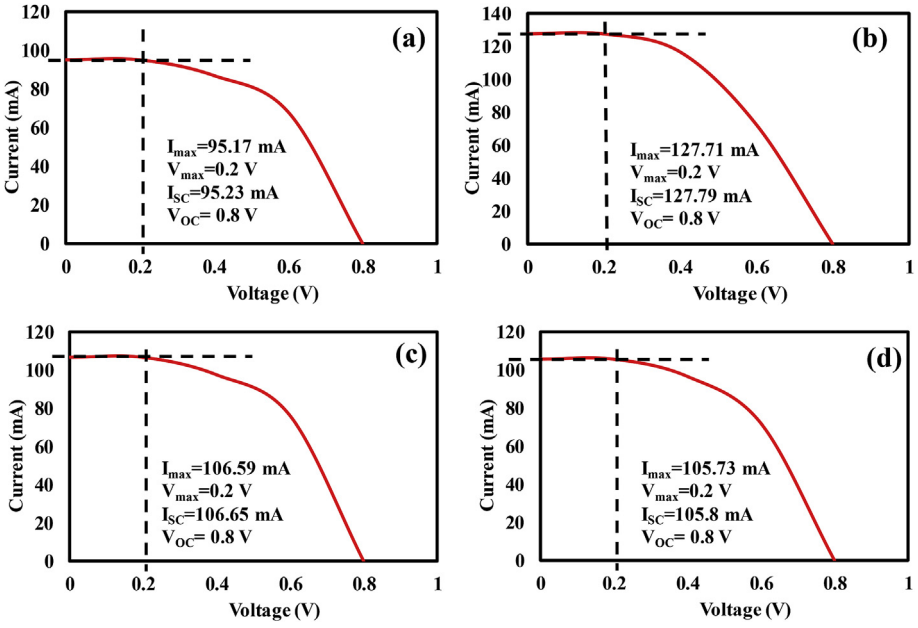

Fig. 12. PV response of (a) 0.5 wt%, (b) 1 wt%, (c) 1.5 wt% and (d) 2 wt% TiO_2 nanoparticles loaded PANi-graphene composites.

In order to improve further the power conversion efficiency of 15 wt % PANi loaded graphene composite, TiO_2 nanoparticles were added in this composite. To obtain again optimized sample with outstanding PV properties, the content of TiO_2 nanoparticles were varied with 0.5–2 wt % by an interval of 0.5 wt%. In this study, 1 wt% TiO_2 nanoparticles loaded PANi-graphene composite shows optimized PV properties. The power conversion efficiency was successfully improved and its value was found to be 8.63%. This is the main accomplishment of present work. In this complete, it is also observed that diode parameters have stable value.

In the concluding remark of this work, it is underlined that concentration of impurity in composite play very important role. Similarly, band gap engineering is also necessary to fabricate more efficient PV cells.

Data availability

The datasets generated during the current study are available from the corresponding author on reasonable request.

Acknowledgements

Authors are very much thankful to Dr. S.K. Omanwar, Head, Department of Physics, Sant Gadge Baba Amravati University, Amravati for providing the facility of Probe Sonicator. Authors are also grateful to Dr. Om Mahodaya, Principal, Jankidevi Bajaj College of Science, Wardha for providing necessary facilities for this work.

Appendix A. Supplementary data

Supplementary data related to this article can be found at https://doi.org/10.1016/j.solidstatesciences.2018.07.009.

References

[1] https://www.bbc.co.uk/education/guides/zpmmmp3/revision.
[2] Y. Liu, X. Wan, F. Wang, J. Zhou, G. Long, J. Tian, J. You, Y. Yang, Y. Chen, Advanced Energy Materials 1 (2011) 771–775.
[3] G. Dennler, M.C. Scharber, C.J. Brabec, Adv. Mater. 21 (2009) 1323–1338.
[4] H.S. Nalwa, Handbook of Organic Conductive Molecules and Polymers, John Wiley & Sons, Chichester, UK, 1997.
[5] E.W. Paul, A.J. Ricco, M.S. Wrighton, J. Phys. Chem. 89 (1985) 1441–1447.
[6] C.R. Kagan, D.B. Mitzi, C.D. Dimitrakopoulos, Science 286 (1999) 945–947.
[7] S.A. Chen, Y. Fang, Synth. Met. 60 (1993) 215–222.
[8] L.D. Pulfry, Photovoltaic Power Generation, Van Nostrand Reinhold Co., New York, 1978.
[9] H.K. Bisoyi, S. Kumar, Liq. Cryst. 38 (2011) 1427–1449.
[10] O. Carp, C.L. Huisman, A. Reller, Prog. Solid State Chem. 32 (2004) 33–177.
[11] D. Dambournet, I. Belharouak, K. Amine, Chem. Mater. 22 (2010) 1173–1179.
[12] E. Singh, H.S. Nalwa, Sci. Adv. Mater. 7 (2015) 1863–1912.
[13] S. Ameen, M.S. Akhtar, G. Kim, Y.S. Kim, O. Yang, H. Shin, J. Alloy. Comp. 487 (2009) 382–386.
[14] L. Shen, W. Guo, H. Xue, Z. Liu, J. Zhou, C. Liu, W. Chen, Proceedings of the 3rd IEEE Int. Conf. on Nano/Micro Engineered and Molecular Systems, January 6-9, (2008) (Sanya, China).
[15] S. Yang, Y. Ishikawa, H. Itoh, Q. Feng, J. Colloid Interface Sci. 356 (2011) 734–740.
[16] S. Zhu, W. Wei, X. Chen, M. Jiang, Z. Zhou, J. Solid State Chem. 190 (2012) 174–179.
[17] M.M. Momeni, M.G. Hosseini, J Mater Sci, Mater Electron 25 (2014) 5027–5034.
[18] A. Bahramian, D. Vashaee, Sol. Energy Mater. Sol. Cells 143 (2015) 284–295.
[19] Y. Duan, Y. Chen, Q. Tang, Z. Zhao, M. Hou, R. Li, B. He, L. Yu, P. Yang, Z. Zhang, J. Power Sources 284 (2015) 178–185.
[20] G. Wang, S. Zhuo, W. Xing, Mater. Lett. 69 (2012) 27–29.
[21] C. Liu, K. Huang, P. Chung, C. Wang, C. Chen, R. Vittal, C. Wu, W. Chiu, K. Ho, J. Power Sources 217 (2012) 152–157.
[22] M. Dinari, M.M. Momeni, M. Goudarzirad, J. Mater. Sci. 51 (2016) 2964–2971.
[23] V. Loryuenyong, S. Yaotrakoo, P. Prathumted, J. Lertsiri, A. Buasri, Micro & Nano Lett. 11 (2016) 77–80.
[24] P. Yang, J. Duan, D. Liu, Q. Tang, B. He, Electrochim. Acta 173 (2015) 331–337.
[25] A.A. Syed, M.K. Dinesan, Talanta 38 (1991) 815–837.
[26] K.R. Nemade, S.A. Waghuley, J. Electron. Mater. 42 (2013) 2857–2866.
[27] T. Salmi, M. Bouzguenda, A. Gastli, A. Masmoudi, Int. J. Renew. Energy Resour. 2 (2012) 213–219.
[28] M. Seifi, A. Soh, N. Izzrib, A. Wahab, M.K.B. Hassan, International Journal of Electrical, Robotics, Electronics Communication Engineering 7 (2013) 97–103.
[29] W. Feng, E. Sun, W.A. Fujii, H.C. Niihara, K. Yoshino, Bull. Chem. Soc. Jpn. 73 (2000) 2627–2632.
[30] Y. Wu, B. Wang, Y. Ma, Y. Huang, N. Li, F. Zhang, Y. Chen, Nano Research 3 (2010) 661–669.
[31] A. Ferrari, J. Robertson, Phys. Rev. B 61 (2000) 14095–14099.
[32] L. Cancado, M. Pimenta, B. Neves, M. Dantas, A. Jorio, Phys. Rev. Lett. 93 (2004) 247401–247405.
[33] A.C. Ferrari, Solid State Commun. 143 (2007) 47–57.
[34] A.C. Ferrari, J. Robertson, Phys. Rev. B 61 (2000) 14095–14107.
[35] R. Wang, Y. Wang, C. Xu, J. Sun, L. Gao, RSC Adv. 3 (2013) 1194–1200.
[36] https://www.e-education.psu.edu/eme812/node/534.
[37] K. Thamaphat, P. Limsuwan, B. Ngotawornchai, J. Kasetsart, Nat. Sci. 42 (2008) 357–361.
[38] K.R. Nemade, S.A. Waghuley, AIP Conference Series 1536 (2013) 1258–1259.
[39] L. Yang, W.W.F. Leung, Adv. Mater. 25 (2013) 1792–1795.
[40] A. Kongkanand, R.M. Dominguez, P.V. Kamat, Nano Lett. 7 (2007) 676–680.